RSC Advances

PAPER

View Article Online
View Journal | View Issue

Cite this: *RSC Adv.*, 2022, **12**, 33449

Self-supporting photocatalyst of 2D Bi_2O_3 anchored on carbon paper for degradation pollutants†

Jianwei Zhou, *[ab] Chubei Wang,[b] Chen Zhou,[c] Fangfang Duo,[b] Liangliang Chu[b] and Mingliang Zhang[b]

Received 25th September 2022
Accepted 18th November 2022

DOI: 10.1039/d2ra06042f

rsc.li/rsc-advances

Two-dimensional vertically aligned Bi_2O_3 nanosheets over carbon paper (CP) were prepared *via* an *in situ* growth approach. Bi_2O_3/CP exhibits a robust photocatalytic activity, as well as renewability and flexibility. With Rhodamine B and 2,4-dichlorophenol used as target pollutants, the rate constant of Bi_2O_3/CP was 3.72×10^{-3} min^{-1} and 6.93×10^{-3} min^{-1} under visible-light irradiation for 2 h, respectively. The improved activity was attributed to the synergistic effects of the hierarchical structure of Bi_2O_3 and the conductive substrate, CP; the former provided efficient catalytic sites for the pollutants and absorbed more of the light scattered among the nanosheets, while the latter is beneficial to the photogenerated electron transfer.

1. Introduction

As one of the most applicable photocatalysis technologies at present, the photocatalytic advanced oxidation process (AOP) has the advantages of strong oxidation capacity, clean energy input, low cost and no secondary pollution, and has been widely applied in the fields of environmental purification, solar energy conversion, biological sterilization, *etc.* Nevertheless, the preparation of highly efficient and widely applicable visible-light responsive photocatalysts still faces many challenges. In recent years, bismuth-based semiconductor materials have been widely applied to the field of optoelectronics.[1,2] As earth-abundance and non-toxic materials, bismuth oxide (Bi_2O_3) semiconductor is an efficient visible-light-driven photocatalyst, which has strong photocorrosion resistance, well chemical stability and catalytic activity.[3–7] However, the intrinsic Bi_2O_3 is mainly limited by the narrow visible-light response range and the rapid recombination of photo-induced electrons (e^-) and holes (h^+) pairs on its surface. Therefore, a lot of research work has been focused on semiconductor modification methods by which Bi_2O_3 can be transformed into a more efficient and robust photocatalyst.[8–11] Because the traditional liquid–solid two-phase photocatalytic reaction systems is still facing the challenge of overall inefficiency, which cannot meet the requirements of commercial application, this urges researchers to constantly seek new reaction systems to enhance the photocatalytic activity.[12,13] Recently, many encouraging new advances have been made in the development of highly efficient gas–liquid–solid three-phase photocatalytic reaction systems.[14,15] It is well known that in the total solar energy spectrum, visible-light and near-infrared light account for about 96%. However, there are still challenges to realize catalytic process under the direct driving of visible light and near-infrared light.[16–20] Although some newly developed narrow-band gap semiconductor photocatalysts can expand the light absorption in the solar spectrum, the enhancement of photocatalytic efficiency is not obvious due to the influence of the e^-–h^+ pairs recombination and the reduction of carrier excited state energy, respectively. Due to the short life of reactive oxygen species (ROSs) and the slow kinetic rate of multi-step free radical reaction in the photocatalytic process, the degradation and mineralization of high concentration aromatic compounds are still a difficulty for the existing photocatalytic system.[21,22]

Compared with semiconductor materials, there are lots of inherent advantages for the photothermal materials such as carbon, boron and noble metals *etc.*, which can absorb low-energy photons and convert them into thermal energy. As a new form of carbon materials, carbon paper with good electrical-conductivity, high temperature resistance, corrosion resistance and smooth surface, has been widely used in material synthesis, electrode materials, catalyst supports and supercapacitors. With special morphology, such as metal nanoparticles, precious metal catalysts, metal sulfides, metal oxides and metal–organic frameworks (MOFs), can be *in situ* synthesized over carbon paper by means of electrochemical

[a]*College of Chemistry and Material Engineering, Xinxiang University, Xinxiang 453003, China. E-mail: jwchow@163.com; Fax: +86-373-3682028; Tel: +86-373-3682028*

[b]*Photoelectrocatalytic Material and Micro-nano Application Technology Academician Workstation, Xinxiang University, Xinxiang 453003, China*

[c]*College of Foreign Languages, Xinxiang University, Xinxiang 453003, China*

† Electronic supplementary information (ESI) available. See DOI: https://doi.org/10.1039/d2ra06042f

deposition or chemical growth approach. A three-phase system of the multifunctional double-layer paper (TiO_2/C) composed of titanium dioxide (TiO_2) and carbon materials was developed at the air–water interface, which also exhibits sunlight-driven catalytic activity and can be conveniently applied to flow photoreactors.[23] The two-dimensional (2D) vertically aligned Sn_3O_4 nanoflakes were successfully prepared over carbon paper *via* hydrothermal process. As a self-powered photoelectrochemical cell-type visible-light detector, Sn_3O_4/CP exhibits flexible and reproducible characteristics and enhanced photosensitivity.[24] AuPt nanoparticles were *in situ* loaded on carbon paper *via* magneto-electro-deposition approach, and the effects of pulse deposition parameters and magnetic field on the catalytic performance were investigated.[25] A novel MoP/Co_2P hybrid structure was anchored on carbon fiber paper by hydrothermal process, and then MoO_2 nanoparticles were deposited *via* chemical vapor deposition (CVD) in the presence of MoO_3, followed by *in situ* phosphating process, which shows higher catalytic activity for hydrogen evolution reaction (HER).[26] With Au, Pd and Pt nanoparticles as basic building blocks, a versatile method was developed for directly growing anisotropic microstructures on 3D carbon paper electrodes. The experimental results show that halides play a crucial role in the morphology of synthesized Au particles, resulting in complex flower-like rough surfaces showing high catalytic activity.[27] Up to now, the reported photocatalytic degradation is usually carried out in discontinuous batch systems with poor stability and scalability. Thus, it is of great significance for applications to construct a highly efficient catalytic system with wide scalability for flow reactor, sunlight irradiation, easy recovery, *etc.*

Herein, a novel self-standing photocatalyst composed of 3D hierarchical Bi_2O_3 single-crystalline nanosheets (NSs) and carbon nanomaterial was developed, in which the Bi_2O_3 NSs were anchored and vertically aligned over the surface of CP. The photocatalytic performance of Bi_2O_3/CP was investigated, and the photocatalytic mechanism was discussed. Bi_2O_3/CP composite can promote the formation of photochemical ROS and enhance the subsequent free radical reaction kinetics in the photocatalytic reaction system, which shows good catalytic oxidation activity under visible-light irradiation. Furthermore, it fully shows the potential of scale-up practical applications.

2. Experimental section

2.1 Materials

All reagents in this study were of analytical grade and without further purification before used. Bismuth(III) nitrate pentahydrate ($Bi(NO_3)_3\cdot 5H_2O$), PEO-PPO-PEO (P123, M_a = 5800), ethylene glycol (EG), Rhodamine B (RhB), 2,4-dichlorophenol (2,4-DCP) and absolute ethanol (C_2H_5OH) were supplied by Sinopharm Chemical Reagent Co., Ltd. Commercial carbon papers were purchased from FuelCellStore.

2.2 Preparation of samples

Prior to deposition, the carbon papers were cut into the required sizes (2.0 cm × 2.0 cm) and repeatedly washed with ethanol, and then dried at 60 °C for 2 hours. The Bi_2O_3/CP composite was formed by *in situ* grown Bi_2O_3 NSs on the carbon paper *via* modified hydrothermal approach using $Bi(NO_3)_3$ as precursors.

Specifically, 2.0 mmol $Bi(NO_3)_3\cdot 5H_2O$ and 0.5 g P123 were added in a mixture solution of ethanol and EG (volume ratio 4 : 1), and then magnetic stirring and ultrasonic treatment for about 1 hour, respectively. The obtained homogeneous solution was transferred to a Teflon-lined autoclave of 50 mL capacity, with the carbon paper vertically immersed in the reaction solution, and kept sealed at 160 °C for 8 hours. After the reaction, the carbon paper coated with a light yellow product was further washed with deionized water and absolute ethanol three times, respectively. The final sample was dried at 60 °C before characterization. For comparison, pure Bi_2O_3 NS was also prepared, and the same experimental conditions were used except the addition of carbon paper.

2.3 Characterization

Morphology analysis was carried on field emission scanning electron microscopy (FESEM, FEI, QUANTA FEG 250). The atomic force microscopy image analysis was conducted with a microscope (AFM, Bruker, Dimension ICON). X-ray diffraction patterns were recorded on X-ray diffractometer (XRD, Cu-K_α radiation, λ = 0.154056 nm, Bruker, D8 Advance). The UV-Vis diffuse reflectance spectra were recorded at room temperature on a spectrophotometer (DRS, Hitachi, U-3010), using $BaSO_4$ as reference. X-ray photoelectron spectroscopy was performed on an electron spectrometer (XPS, Al K_α, $h\nu$ = 1486.6 eV, Thermo Fisher, Escalab xi+), with the signal of C 1s peak at 284.8 eV as reference. Using 150 W Xe lamp as the excitation light source, photoluminescence spectra analysis was carried out on the fluorescence spectrometer (PL, Hitachi, F-4600) and the excitation wavelength was 320 nm. Using an electrochemical system (CHI-660B, China), the transient photocurrent response was measured with a standard three-electrode system, a standard calomel electrode (SCE) as the reference electrode, 0.1 M Na_2SO_4 as the electrolyte solution and 300 W Xe lamp as light source.

2.4 Photocatalytic performance evaluation

500 W Xe lamp (the emission λ_{max} = 470 nm and light intensity about 150 mW cm^{-2}) with 400 nm cutoff filter as visible-light source, the photocatalytic reaction was performed in a XPA photoreaction apparatus. The temperature of the reaction solution is maintained at approximately 25 °C. The aqueous solutions of RhB (1×10^{-5} mol L^{-1}) and 2,4-DCP (10 mg L^{-1}) were used as model pollutant, respectively. In the typical process, a certain amount of as-prepared catalysts were added into the 50 mL solution of pollutant in a quartz tube reactor for ultrasound treating 10 minutes. Prior to irradiation, the suspensions were kept stirring for 30 minutes in darkness to achieve adsorption–desorption equilibrium. And then, the photocatalytic reaction was carried out with a sampling interval of 30 minutes. The suspended catalyst particles were separated by centrifugation at 8000 rpm for 10 minutes and the

absorbance of supernatant was measured on the UV-Vis spectrophotometer. No catalyst was added in blank test under and the same conditions.

The first-order kinetic reaction rate constant (k values) of photocatalytic system was calculated as follows equation.

$$-\ln\left(\frac{C_i}{C_0}\right) = kt$$

where C_0 and C_i refer to the concentration of pollutants before and after irradiation, t is the reaction time.

2.5 Active species trapping tests

To detect the active species during the photocatalytic reaction process, hydroxyl radicals ($\cdot$OH), superoxide radical ($\cdot O_2^-$) and holes (h^+) were investigated by adding 1.0 mmol *tert*-butanol (TBA, a quencher for $\cdot$OH), 1.0 mmol *p*-benzoquinone (PBQ, a quencher for $\cdot O_2^-$) or 1.0 mmol disodium ethylenediamine tetraacetate (EDTA-2Na, a quencher for h^+), respectively. The experimental test was similar to the former photocatalytic performance test process.

3. Results and discussion

3.1 Structure and performance characterization

The scanning electron microscope (SEM) images were shown in Fig. 1. In order to clearly see the growth process of Bi_2O_3 NSs on carbon paper, the SEM images of the original carbon paper and the low and high-magnification SEM images of the Bi_2O_3 NSs over carbon paper were shown in Fig. 1. As can be seem from Fig. 1a and b, carbon paper clearly shows the micro-porous layer on the surface of carbon paper, which has good permeability and is also conducive to the diffusion of O_2 molecules through carbon paper in solution. In the Fig. 1c and d, it can be found that Bi_2O_3 NSs were vertically grown on the surface of carbon paper in a hierarchical structure, and the vertically aligned Bi_2O_3 NSs were densely and uniformly distributed on the surface of carbon paper. The thickness of each Bi_2O_3 NS was ultra-thin and translucent, with the diameter about 800–1000 nm, which were crossover connected to form a porous structure with the size range of mesoporous grade.

Crystal phase structure analysis of the samples was shown in the XRD pattern. In Fig. 2a, three diffraction peaks were observed at diffraction angles 2θ of 18.1°, 26.5° and 54.8° derived from the carbon substrate, which were attributed to the characteristic peaks of carbon paper material. The crystalline structure of Bi_2O_3 was identified from the XRD patterns in Fig. 2b. The peaks of the Bi_2O_3 was regarded as monoclinic phase Bi_2O_3 (JCPDS no. 41-1449), and the major peaks at $2\theta = 28.3°$, 32.6°, and 46.8° well match the (120), (121) and (041) planes. Moreover, except the peak of α-Bi_2O_3, no new diffraction peaks were observed in the XRD spectrum of Bi_2O_3/CP, which can be attributed to the growth of pure Bi_2O_3 NSs covered on the surface of carbon paper.

XPS analysis was performed to investigate the elemental composition, chemical state and molecular structure of the Bi_2O_3/CP composite surface. Seen from the survey spectra in Fig. 2c, the result indicates the presence of Bi, O, and C atoms in the composite sample, which is in accordance with the bulk composition of Bi_2O_3/CP. High resolution XPS spectra of Bi 4f, O

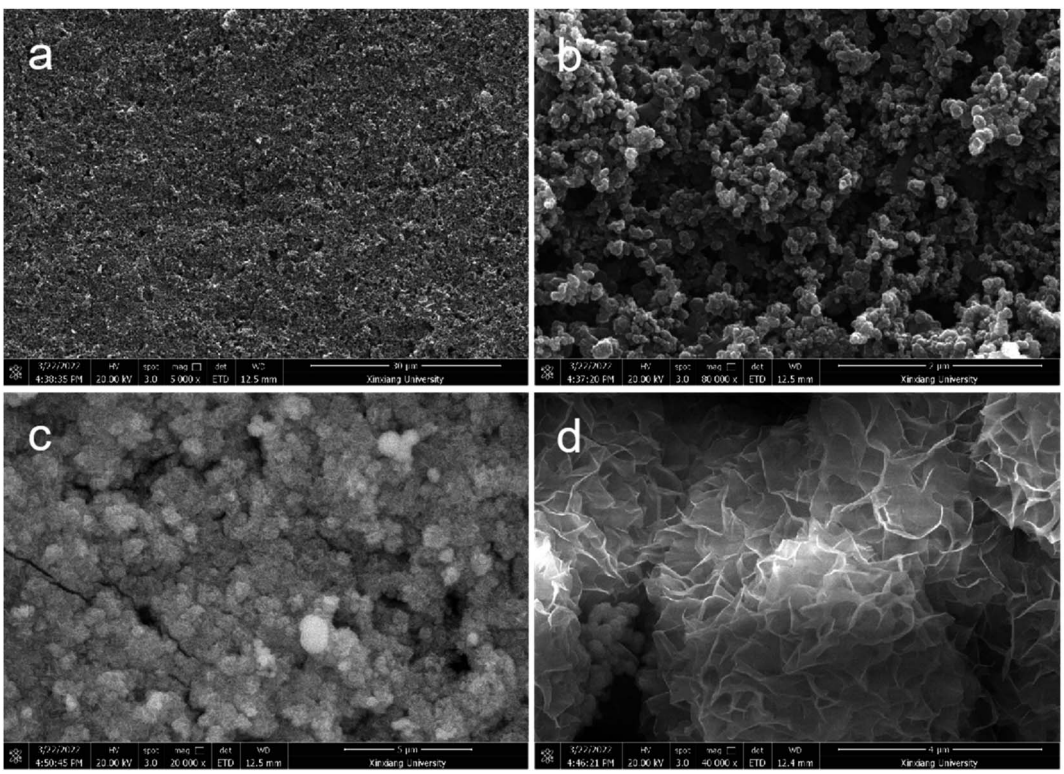

Fig. 1 Low-magnification and magnified SEM images of the CP (a, b) and the Bi_2O_3 structure consisted of nanoplate building blocks (c, d).

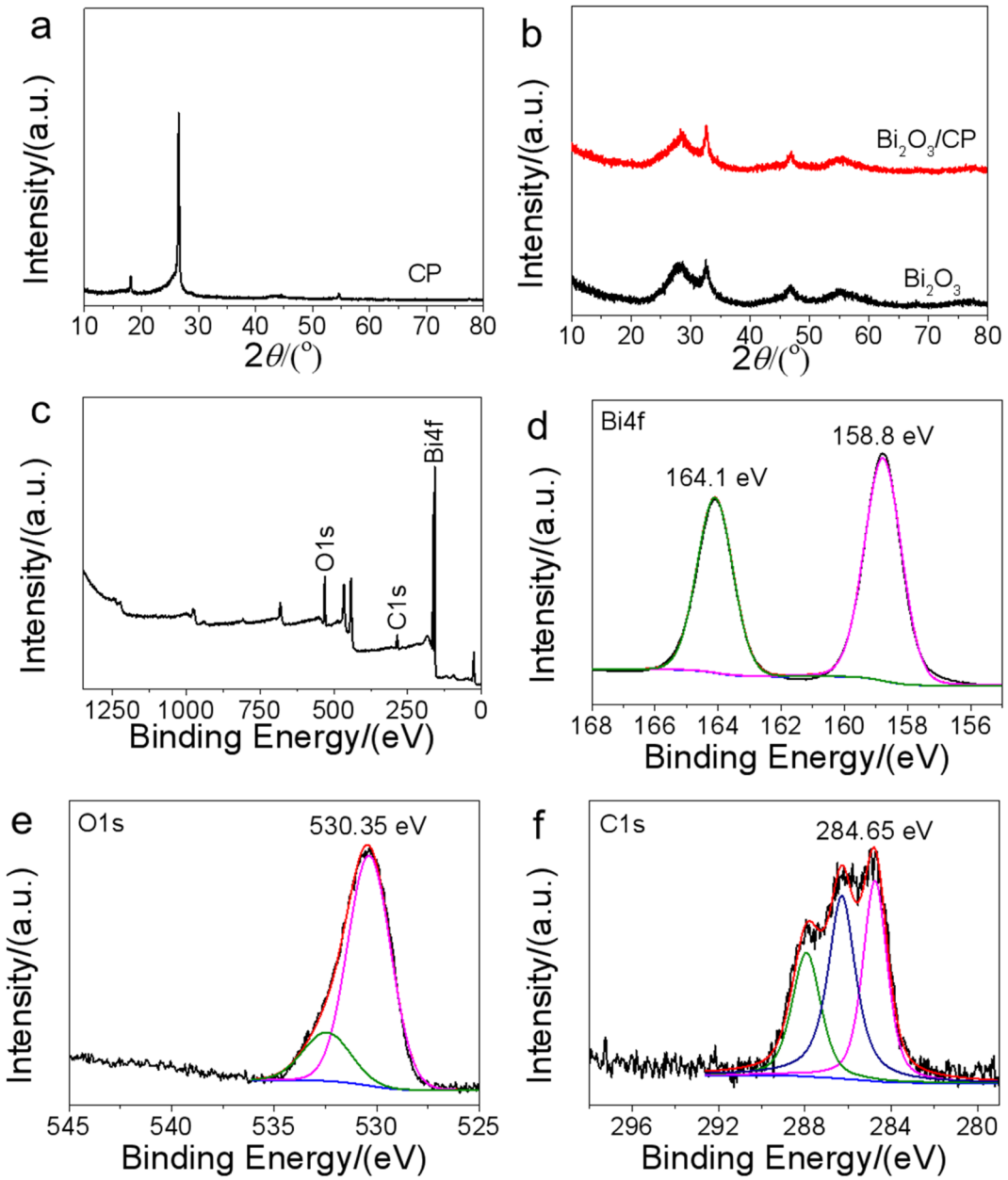

Fig. 2 XRD patterns of CP (a), Bi_2O_3 and Bi_2O_3/CP (b), XPS survey spectra of Bi_2O_3/CP (c) and high-resolution XPS spectra of Bi 4f (d), O 1s (e) and C 1s (f).

1s and C 1s were shown in Fig. 2. For pure Bi_2O_3 sample, the binding energies (BE) of 164.0 eV and 158.7 eV were attributed to Bi $4f_{5/2}$ and Bi $4f_{7/2}$ orbitals, respectively, which was in consistent with the reported previously.[28] For Bi_2O_3/CP composite in Fig. 2d, the BEs of Bi $4f_{5/2}$ and Bi $4f_{7/2}$ shown a slight positive shift at 164.1 eV and 158.8 eV, respectively, indicating decreased electron density of Bi in the Bi_2O_3/CP, which may be due to electron transfer from Bi_2O_3 to CP, suggesting that there is a strong interface interaction between Bi_2O_3 and CP. In the case of Bi_2O_3/CP composite, the BE of O 1s shows a slight positive shift at 530.35 eV in Fig. 2e. The O 1s peak of Bi_2O_3 at 529.7 eV is associated with the O^{2-} in Bi_2O_3.[29] This may be attributed to the adsorbed oxygen on the surface of Bi_2O_3/CP composite. The high-resolution C 1s spectra in Fig. 2f can be deconvoluted into three dominant peaks with binding energies of 284.65 eV, 286.25 eV and 287.95 eV. The peaks at 286.25 and 284.65 eV are identified as the typical C–C bonds of CP and/or adventitious carbon species of Bi_2O_3/CP, respectively. And that peak at 287.95 eV can be assigned to the sp^2-hybridized carbon in the CP. Compared with the C 1s peak at 284.8 eV is attributed to the adventitious carbon, in the C 1s spectrum of Bi_2O_3/CP, the BE at 284.65 eV shows a negative shift, indicating that the electron density of carbon atoms in CP was increased. Combined with the blue shift in Bi 4f BE and red shift in C 1s BE increases, it can be concluded that the migration direction of electrons on Bi_2O_3/CP heterostructure interface is from the conduction band of Bi_2O_3

semiconductor to the surface of conductive CP. The results of XPS analysis suggested that a close heterostructure was formed between Bi_2O_3 and CP through strong interaction rather than the simple physical stacking.

In this study, Bi_2O_3 NSs were *in situ* grown onto carbon paper. A layer CP photograph (size: 25 cm × 20 cm) in the Fig. 3a, Bi_2O_3/CP bilayer after Bi_2O_3 NS immobilization on the CP and the cross-sectional scanning images can be shown in Fig. 3b. According to Fig. 3c, the cross-sectional scanning image shows that the CP is designed to have single side wettability. Besides, the Bi_2O_3 layer side is hydrophilic and exhibits a water contact angle of 7° in Fig. 3d and inset. The Bi_2O_3 NSs layer with a certain thickness was fixed onto the CP surface, combining with abundant porous structures. It is well known that the morphology and interfacial wettability of catalyst layer plays a vital role in regulating the mass transfer for reactants at the two-phase interface. Thus, the wettability and the porous structure can effectively transfer oxygen and pollutant molecules from liquid phases to the surface of Bi_2O_3 photocatalysts, respectively.

In order to investigate the optical properties of the obtained photocatalysts, the UV-Vis diffuse reflectance spectra (DRS) of as-prepared samples were also investigated. As can be seen from Fig. 4a, the steep absorption edge of Bi_2O_3 is about 442 nm, and the Bi_2O_3/CP shows absorption wavelengths from the UV to the visible range up to 460 nm. Compared with the sole Bi_2O_3, the absorption edge of the Bi_2O_3/CP composite shows enhanced visible-light absorption. In addition, it was revealed in Fig. 4b of the optical absorption edge of the Bi_2O_3/CP heterostructure (E_g = 2.7 eV) and bare Bi_2O_3 (E_g = 2.8 eV), which displayed obvious red shift compared with the bare Bi_2O_3. This may be attributed to the interaction between Bi_2O_3 and CP interfaces in the Bi_2O_3/CP heterostructure. The enhanced visible-light absorption indicates that Bi_2O_3/CP can produce more photogenerated carriers, which will be favorable for photocatalytic reaction.

3.2 Photocatalytic activity

Firstly, the catalytic activities of as-prepared samples were evaluated *via* the degradation of 2,4-DCM under the visible-light irradiation. The photodecomposition of 2,4-DCM without photocatalyst could not be observed from Fig. 5a, indicating its own very stability. The degradation curves of 2,4-DCM aqueous solution over Bi_2O_3 and Bi_2O_3/CP is shown in the Fig. 5a, and the obvious increase of the degradation rate that indicates the effective degradation of 2,4-DCM on the Bi_2O_3/CP. Under visible-light irradiation (λ > 400 nm), the first-order kinetics of photocatalytic reaction was investigated experimentally. As shown from Fig. 5b, Bi_2O_3/CP composite ($k = 6.93 \times 10^{-3}$ min^{-1}) reflected higher photocatalytic activity than the sole Bi_2O_3 ($k = 5.0 \times 10^{-3}$ min^{-1}). The enhanced photocatalytic activity of the Bi_2O_3/CP composite suggests beneficial roles of forming a tight contact heterostructured between Bi_2O_3 and CP components, in addition to the effects of light absorption or specific surface area. The photocatalytic degradation of RhB could be also observed from

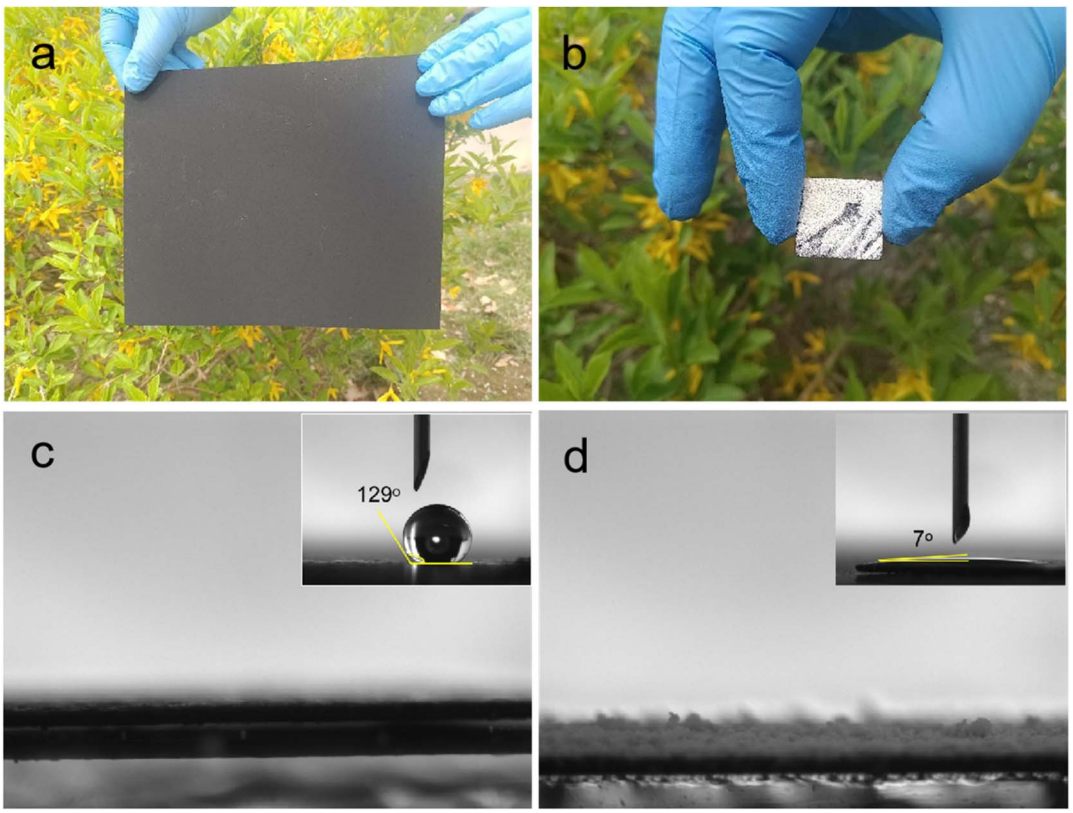

Fig. 3 Photograph of a piece CP (a), top-view images of Bi_2O_3/CP bilayer CP (2 cm × 2 cm) (b), side-view images of CP (c) and CP after Bi_2O_3 immobilization (d), insets in show the water-droplet on each layer structure.

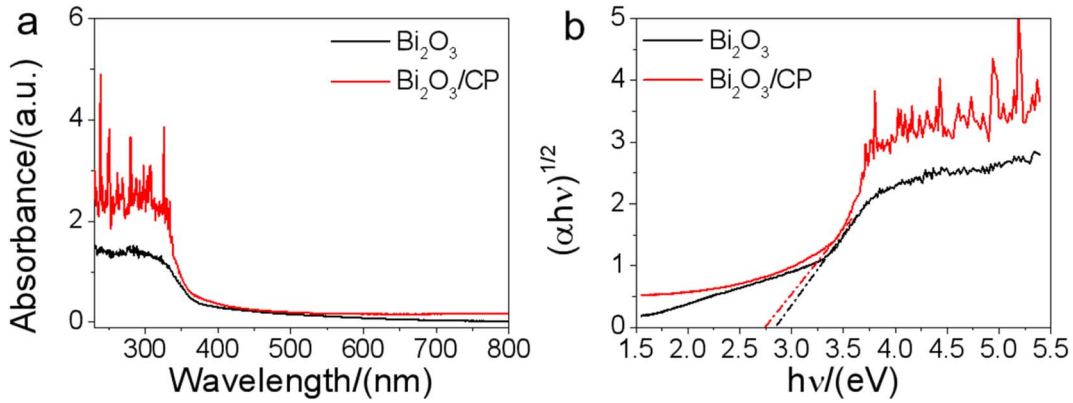

Fig. 4 UV-Vis diffuse reflectance spectra (a) and the optical absorption edges (b) of the Bi_2O_3 and Bi_2O_3/CP.

Fig. 5c and d. Bi_2O_3/CP composite has high photocatalytic activity, which rate constant value ($k = 3.72 \times 10^{-3}$ min^{-1}) is about 1.7 times that of bare Bi_2O_3 ($k = 2.12 \times 10^{-3}$ min^{-1}). The experimental results show that Bi_2O_3/CP composite exhibits better photocatalytic performance than pure Bi_2O_3 NS under visible-light irradiation.

3.3 Investigation on photocatalytic mechanism and durability

The mechanism of enhancing photocatalytic activity was studied by means of photocurrent analyses, photoluminescence analyses and reactive species trapping experiments, *etc.* Fig. 6a displays the transient photocurrent response (TPR) of Bi_2O_3/CP and Bi_2O_3 NS under visible-light irradiation, respectively. In semiconductor mediated photocatalytic reactions, the effective separation of e^-–h^+ pairs and the successful migration of photogenerated carriers to the surface play a crucial role. The transient photocurrent response originates from the directional diffusion of photoelectrons, which reflects the separation efficiency of photogenerated carriers. In order to investigate the transition of photogenerated electrons in Bi_2O_3 NS before and after carbon paper modification, photoelectrochemical measurement was carried out to clarify the interfacial charge transfer dynamics between Bi_2O_3 semiconductor and carbon

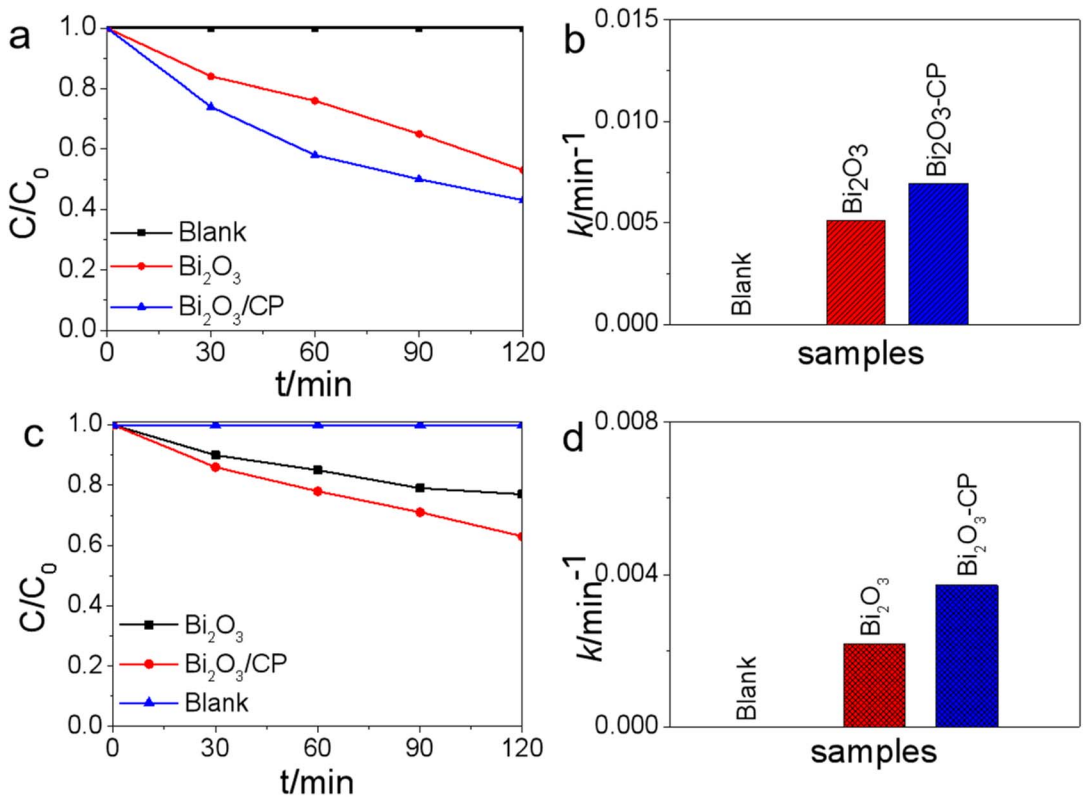

Fig. 5 The degradation curves (a) and reaction rate constant (b) of 2,4-DCP and the degradation curves (c) and reaction rate constant (d) of RhB under visible-light (λ > 400 nm) irradiation, respectively.

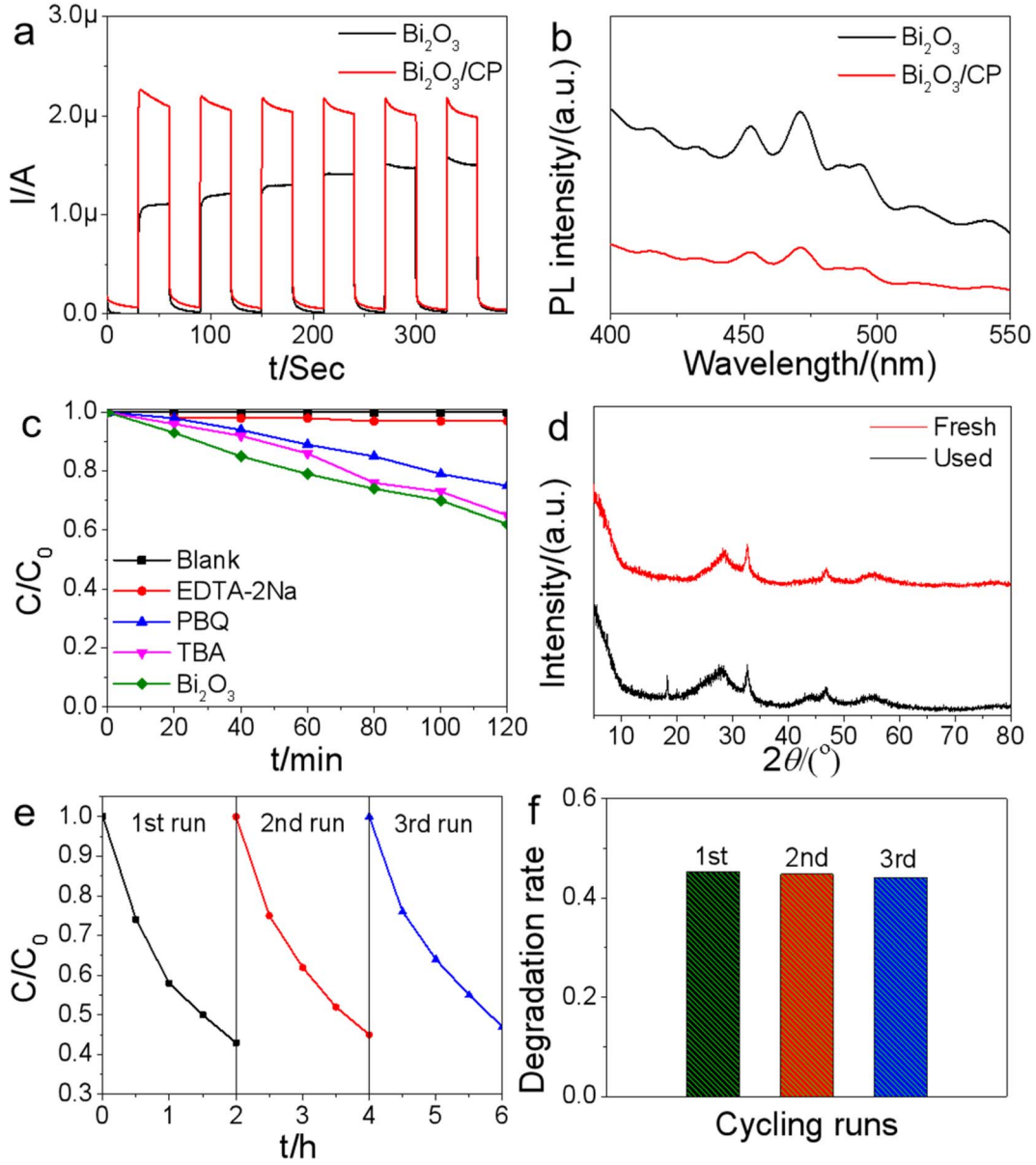

Fig. 6 Photocurrent profiles of Bi_2O_3 and Bi_2O_3/CP under visible-light irradiation (a), PL spectra of Bi_2O_3 and Bi_2O_3/CP with the 150 W Xe lamp excitation light source (b), effects of reactive species scavengers on the RhB degradation performance of Bi_2O_3/CP (c), XRD patterns of fresh and used 3 times Bi_2O_3/CP samples (d), cycles of 2,4-DCP degradation (e) and RhB degradation (f) over Bi_2O_3/CP photocatalysis.

paper. It can be observed from Fig. 6a that the photocurrent intensity of Bi_2O_3/CP composite shows remarkably higher than that of single Bi_2O_3, implying that separation efficiency of the photogenerated e^-–h^+ pairs is improved and more photoinduced carriers can be generated, which is conducive to enhancing the photocatalytic activity of Bi_2O_3/CP.

The spatial directional separation of carriers is one of the most important factors for the effective utilization of photogenerated carriers. Moreover, reducing the recombination rate of photogenerated e^-–h^+ pairs is the key to improve the photocatalytic activity. In this paper, the recombination of photogenerated carriers was also estimated by PL spectroscopy, and the PL spectra of Bi_2O_3 and Bi_2O_3/CP were measured under the excitation wavelength of 320 nm. By contrast, the spectra of Bi_2O_3 with strong emission at 470 nm could be observed in the Fig. 6b. The emission peak intensity of Bi_2O_3 is stronger than that of Bi_2O_3/CP composite, which decrease in PL intensity of Bi_2O_3/CP is ascribed to electron migration from Bi_2O_3 semiconductor to CP, according to a Schottky junction scheme, resulting in enhanced photogenerated e^-–h^+ pairs effective spatial separation on Bi_2O_3 semiconductor.

In order to deeply understand the mechanism of photocatalytic reaction, it is necessary and important to investigate the reactive species in the photocatalytic process. In terms of photocatalysis, there may be many active species in the process of photocatalysis, including h^+, $\cdot OH$ and $\cdot O_2^-$ *etc.* As can be

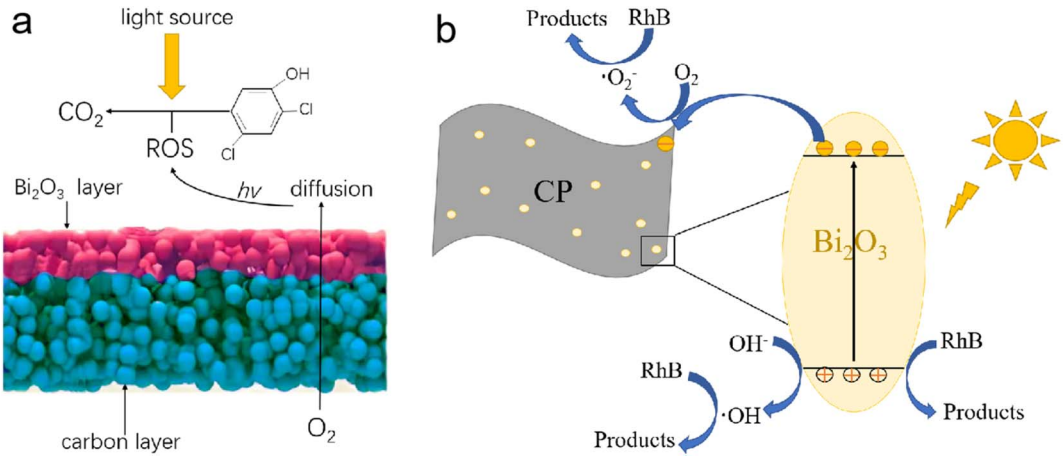

Fig. 7 Schematic illustration for photocatalytic oxidation degradation 2,4-DCM (a), and proposed mechanism for the photocatalytic degradation of RhB on the Bi_2O_3/CP composites (b).

shown in Fig. 6c, the photocatalytic activity of Bi_2O_3/CP composite was greatly suppressed by the addition of EDTA-2Na, suggesting that h^+ was the main reactive species. Similarly, the obvious decrease in the photocatalytic activity observed by the addition of PBQ radical scavenger, suggested that $\cdot O_2^-$ radical play an important role in the reaction, too. However, while the addition of TBA radical scavenger had weakest effects in reducing the activity, demonstrating that ·OH radical given play to an insignificant role in the photocatalytic reaction over Bi_2O_3/CP surface.

In addition to thinking over the photocatalytic efficiency of catalysts, the stability is also very critical and important for practical application. As shown XRD patterns in Fig. 6d, the crystal structure of Bi_2O_3/CP catalyst remains unchanged and there is no photocorrosion after 3 cycling runs in 6 h, which indicate that the Bi_2O_3/CP composite possess good reusability for photocatalytic applications. To evaluate the durability and efficiency of the photocatalytic performance of Bi_2O_3/CP composite in the process of photocatalytic reaction, the recycling tests of the photocatalytic degradation were also carried out. As can be shown in Fig. 6e and f, the degradation efficiency of 2,4-DCP and RhB did not show a distinct attenuation after three cycles with the same photocatalyst. The as-prepared Bi_2O_3/CP composite had high activity and stability in the degradation process under visible-light irradiation, so it can be considered that Bi_2O_3/CP is a relatively stable photocatalyst.

The increased catalytic activity of the as-prepared Bi_2O_3/CP photocatalyst could be attributed to the enhancement of the visible-light absorption, the efficient separation and easy transfer of photoinduced e^-–h^+ pairs. Such as C_3N_4/$BiPO_4$ and other covering structures,[30] the Bi_2O_3/CP composite structure is considered to be conducive to the electron transport between individual Bi_2O_3 and CP, driven by interface synergy effect. A possible photocatalytic mechanism of the Bi_2O_3/CP composites is schematically illustrated in Fig. 7a. The self-standing Bi_2O_3/CP composites in the water body with Bi_2O_3 NSs layer upward to form a liquid–solid two-phase heterostructure, and the visible-light source was irradiated from the top of this catalytic system. Oxygen molecules (O_2) can diffuse from liquid-phase to the surface of Bi_2O_3 semiconductor through the porous CP substrate, followed generation to ROSs *via* the photocatalytic reduction. Then, in the liquid-phase, the organic pollutant molecules will be degraded by successive radical reactions and finally mineralized into inorganic carbon (CO_2) and water molecules (H_2O).[31]

As shown in Fig. 7b, the reactive species of $\cdot O_2^-$ and ·OH free radicals could be generated over Bi_2O_3 NS semiconductor surface *via* redox reaction pathway $O_2 + e^- \rightarrow \cdot O_2^-$ (conduction band, CB) and $OH^- + h^+ \rightarrow \cdot OH$ (valence band, VB), respectively. Due to the effective photoinduced electrons transfer from the CB of Bi_2O_3 semiconductor to the CP *via* the interfaces, the recombination rate of e^-–h^+ pairs was decreased, and more reactive species of $\cdot O_2^-$ and ·OH free radicals could be formed to enhance the photocatalytic efficiency under the visible-light irradiation. Besides, the introduction of CP carbon materials enhances the visible-light absorption of Bi_2O_3 semiconductors, so that can produce extra photogenerated electrons and holes, and is be beneficial for its better catalytic activity. Synergistic effect of improving the photogenerated charges migration dynamics and reducing the recombination probability of e^-–h^+ pairs could be found in the Bi_2O_3/CP photocatalyst. The photogenerated electrons can quickly inject into electroconductive carbon paper, which effectively retards the recombination of e^-–h^+ pairs in the Bi_2O_3 semiconductor and enhances the efficiency of surface photocatalytic reaction dynamics.

4. Conclusions

Using Bi_2O_3 semiconductors and carbon papers as raw materials, a scalable Bi_2O_3/CP photocatalyst was successfully fabricated by means of a facile *in situ* liquid phase grown approach. In the photocatalytic reaction system, self-standing at liquid–solid interfaces for photocatalysis was developed, and the photoinduced production of ROSs can be facilitated *via* rapid oxygen diffusion at the two-phase interfaces, while the interfacial effect promotes the effective separation of photogenerated

e^-–h^+ pairs and the following radical reactions over the Bi_2O_3/CP surface for AOP of RhB and 2,4-DCP. Compared with Bi_2O_3 powders dispersed system, the Bi_2O_3/CP exhibited better visible-light photocatalytic activity, owning to the synergistic effect of interfacial charges migration between Bi_2O_3 semiconductor and conductive CP substrate. In photocatalytic water purification applications, Bi_2O_3/CP composites also show high stability and the feasibility of sunlight driven, showing the potential for large-scale efficient degradation of organic pollutants.

Author contributions

Jianwei Zhou: conceptualization, data curation, formal analysis, writing – original draft. Chubei Wang: writing – review & editing. Chen Zhou: Writing – review & editing. Fangfang Duo: investigation, writing – review & editing. Liangliang Chu: writing – review & editing. Mingliang Zhang: writing – review & editing. All the authors discussed the results and contributed to the work.

Conflicts of interest

The authors declare no conflict of interest.

Acknowledgements

This work is supported by the Project of Science and Technology of the Henan province (192102310496).

References

1 F. Amano, A. Yamakata, K. Nogami, M. Osawa and B. Ohtani, Visible light responsive pristine metal oxide photocatalyst: enhancement of activity by crystallization under hydrothermal treatment, *J. Am. Chem. Soc.*, 2008, **130**, 17650–17651.

2 H. R. An, S. W. Cao and J. G. Yu, Recent advances in morphology control and surface modification of Bi-based photocatalysts, *Acta Phys. Chim. Sin.*, 2016, **32**, 2841–2870.

3 R. A. He, J. Q. Zhou, H. Q. Fu, S. Y. Zhang and C. J. Jiang, Room-temperature in situ fabrication of Bi_2O_3/g-C_3N_4 direct Z-scheme photocatalyst with enhanced photocatalytic activity, *Appl. Surf. Sci.*, 2018, **430**, 273–282.

4 L. S. Zhang, W. Z. Wang, J. Yang, Z. G. Chen, W. Q. Zhang, L. Zhou and W. Liu, Sonochemical synthesis of nanocrystallite Bi_2O_3 as a visible-light-driven photocatalyst, *Appl. Catal. Gen.*, 2006, **308**, 105–110.

5 M. Xiong, L. Chen, Q. Yuan, J. He, S. L. Luo, C. T. Au and S. F. Yin, Controlled synthesis of graphitic carbon nitride/beta bismuth oxide composite and its high visible-light photocatalytic activity, *Carbon*, 2015, **86**, 217–224.

6 Y. Huang, W. Wang, Q. Zhang, J. J. Cao, R. J. Huang, W. Ho and S. C. Lee, In situ fabrication of α-Bi2O3/(BiO)2CO3 nanoplate heterojunctions with tunable optical property and photocatalytic activity, *Sci. Rep.*, 2016, **6**, 23435–23444.

7 Z. H. Ai, Y. Huang, S. C. Lee and L. Z. Zhang, Monoclinic α-Bi_2O_3 photocatalyst for efficient removal of gaseous NO and HCHO under visible light irradiation, *J. Alloys Compd.*, 2011, **509**, 2044–2049.

8 D. P. Dutta, M. Roy and A. K. Tyagi, Dual function of rare earth doped nano Bi_2O_3: white light emission and photocatalytic properties, *Dalton Trans.*, 2012, **41**, 10238–10248.

9 S. C. Sun, X. P. Jiang, W. Xiao, Y. F. Jiang, W. M. Zhou, I. Lawan, M. X. Zhang, Z. N. Garba, L. W. Wang and Z. H. Yuan, A simple method for construction of Bi_2O_3/$Bi_6O_6(OH)_3(NO_3)_3 \cdot 1.5H_2O$ p–n junction photocatalyst with superior photocatalytic performance, *Mater. Lett.*, 2020, **276**, 128199–128207.

10 Y. X. Li, M. M. Wen, Y. Wang, G. Tian, C. Y. Wang and J. C. Zhao, Plasmonic hot electrons from oxygen vacancies for infrared light-driven catalytic CO_2 reduction on Bi_2O_{3-x}, *Angew. Chem., Int. Ed.*, 2021, **133**, 923–929.

11 H. J. Lu, Q. Hao, T. Chen, L. H. Zhang, D. M. Chen, C. Ma, W. Q. Yao and Y. F. Zhu, A high- performance Bi_2O_3/Bi_2SiO_5 p-n heterojunction photocatalyst induced by phase transition of Bi_2O_3, *Appl. Catal. B Environ.*, 2018, **237**, 59–67.

12 W. Fan, B. Zhang, X. Wang, W. Ma, D. Li, Z. Wang, M. Dupuis, J. Shi, S. Liao, C. Li, W. J. Fan, B. Q. Zhang, X. Y. Wang, W. G. Ma, D. Li, Z. L. Wang, M. Dupuis, J. Y. Shi, S. J. Liao and C. Li, Efficient hydrogen peroxide synthesis by metal-free polyterthiophene *via* photoelectron-catalytic dioxygen reduction, *Energy Environ. Sci.*, 2020, **13**, 238–245.

13 R. Long, Y. Li, Y. Liu, S. M. Chen, X. S. Zheng, C. Gao, C. H. He, N. S. Chen, Z. M. Qi, L. Song, J. Jiang, J. F. Zhu and Y. J. Xiong, Isolation of Cu atoms in Pd lattice: forming highly selective sites for photocatalytic conversion of CO_2 to CH_4, *J. Am. Chem. Soc.*, 2017, **139**, 4486–4492.

14 A. Li, Q. Cao, G. Y. Zhou, B. Schmidt, W. J. Zhu, X. T. Yuan, H. L. Huo, J. L. Gong and M. Antonietti, Three-phase photocatalysis for the enhanced selectivity and activity of CO_2 reduction on hydrophobic surface, *Angew. Chem., Int. Ed.*, 2019, **58**, 14549–14555.

15 L. P. Chen and X. J. Feng, Enhanced catalytic reaction at an air–liquid–solid triphase interface, *Chem. Sci.*, 2020, **11**, 3124–3131.

16 Q. Shi and J. Ye, Deracemization enabled by visible-light photocatalysis, *Angew. Chem., Int. Ed.*, 2020, **59**, 4998–5001.

17 R. J. Feng, W. Y. Lei, G. Liu and M. H. Liu, Visible- and NIR-light responsive black-phosphorus-based nanostructures in solar fuel production and environmental remediation, *Adv. Mater.*, 2018, **30**, 1804770–1804779.

18 L. Tian, J. Y. Li, F. Liang, J. K. Wang, S. S. Li, H. J. Zhang and S. W. Zhang, Molten salt synthesis of tetragonal carbon nitride hollow tubes and their application for removal of pollutants from wastewater, *Appl. Catal. B Environ.*, 2018, **225**, 307–313.

19 F. Liang, L. Tian, H. J. Zhang, F. Liang, S. M. Liu, R. S. Cheng and S. W. Zhang, Low temperature synthesis of $LiSi_2N_3$ nanobelts via molten salt nitridation and their photoluminescence properties, *RSC Adv.*, 2016, **6**, 68615–68618.

20 Z. J. Gong, T. Ma and F. Liang, Syntheses of magnetic blackberry-like Ni@Cu@Pd nanoparticles for efficient catalytic reduction of organic pollutants, *J. Alloys Compd.*, 2021, **873**, 159802–159812.

21 D. X. Li, J. C. C. Yu, V. H. Nguyen, J. C. S. Wu and X. X. Wang, A dual-function photocatalytic system for simultaneous separating hydrogen from water splitting and photocatalytic degradation of phenol in a twin-reactor, *Appl. Catal. B Environ.*, 2018, **239**, 268–279.

22 Z. H. Mo, K. Wang, H. Yang, Z. Q. Ou, Y. X. Tong, T. W. Yu, Y. Wang, P. Tsiakaras and S. Q. Song, Heterojunction architecture of pTTh nanoflowers with CuOx nanoparticles hybridized for efficient photoelectrocatalytic degradation of organic pollutants, *Appl. Catal. B Environ.*, 2020, **277**, 119249–119258.

23 H. N. Huang, R. Shi, X. R. Zhang, J. Q. Zhao, C. L. Su and T. R. Zhang, Photothermal-assisted triphase photocatalysis over a multifunctional bilayer paper, *Angew. Chem., Int. Ed.*, 2021, **60**, 22963–22969.

24 W. W. Xia, H. Y. Qian, X. H. Zeng, J. Dong, J. Wang and Q. Xu, Visible light self-powered photodetectors and recoverable photocatalyst fabricated from vertically aligned Sn_3O_4 nanoflakes on carbon paper, *J. Phys. Chem. C*, 2017, **121**, 19036–19043.

25 J. Q. Zhang, D. Li, M. M. Chen, M. Z. An, P. X. Yang and P. Wang, Effect of magnetic field on properties of AuPt particles magnetoelectrodeposited on carbon paper, *Chin. J. Chem. Phys.*, 2014, **27**, 704–710.

26 P. P. Zhou, Y. Q. Zhang, B. Ye, S. Qin, R. R. Zhang, T. Y. Chen, H. J. Xu, L. Zheng and Q. H. Yang, MoP/Co_2P hybrid nanostructure anchored on carbon fiber paper as an effective electrocatalyst for hydrogen evolution, *ChemCatChem*, 2019, **11**, 6086–6091.

27 Y. Holade, D. P. Hickey and S. D. Minteer, Halide-regulated growth of electrocatalytic metal nanoparticles directly onto a carbon paper electrode, *J. Mater. Chem. A*, 2016, **4**, 17154–17162.

28 S. Shamaila, A. K. L. Sajjad, F. Chen and J. L. Zhang, Study on highly visible light active Bi_2O_3 loaded ordered mesoporous titania, *Appl. Catal. B Environ.*, 2010, **94**, 272–280.

29 S. Balachandran and M. Swaminathan, Facile fabrication of heterostructured Bi_2O_3-ZnO photocatalyst and its enhanced photocatalytic activity, *J. Phys. Chem. C*, 2012, **116**, 26306–26312.

30 C. S. Pan, J. Xu, Y. J. Wang, D. Li and Y. F. Zhu, Dramatic activity of $C_3N_4/BiPO_4$ photocatalyst with core/shell structure formed by self-assembly, *Adv. Funct. Mater.*, 2012, **22**, 1518–1524.

31 G. Litwinienko and K. U. Ingold, Solvent effects on the rates and mechanisms of reaction of phenols with free radicals, *Acc. Chem. Res.*, 2007, **40**, 222–230.